Characterizing the Local Variations of the Northern Australian Rainy Season

JOHN UEHLING,[a,b] VASUBANDHU MISRA,[a,b,c] AMIT BHARDWAJ,[b,c,d] AND NIRUPAM KARMAKAR[e,f]

[a] *Department of Earth, Ocean, and Atmospheric Science, Florida State University, Tallahassee, Florida*
[b] *Center for Ocean-Atmospheric Prediction Studies, Florida State University, Tallahassee, Florida*
[c] *Florida Climate Institute, Florida State University, Tallahassee, Florida*
[d] *Numerical Weather Prediction, India Meteorological Department, Ministry of Earth Sciences, New Delhi, India*
[e] *Indian Institute of Tropical Meteorology, Pune, Maharashtra, India*
[f] *National Centre for Medium Range Weather Forecasting, Ministry of Earth Sciences, Government of India, Noida, Uttar Pradesh, India*

(Manuscript received 3 May 2021, in final form 13 September 2021)

ABSTRACT: In this study, we introduce a localized definition of the onset and retreat of the northern Australian rainy season that is solely based on gridded rainfall analysis. Our analysis shows that the local onset/retreat of the rainy season has considerable spatial heterogeneity. Onset is earlier and the length of the rainy season is longer to the west of the Gulf of Carpentaria than to its east. Furthermore, we also find the local onset/retreat is influenced by the wet and dry spells of the 30–60-day intraseasonal oscillation. Much of the retreat of the rainy season occurs in the dry phases of the intraseasonal oscillation. However, intriguingly, a majority of the local onset of the rainy season occurs during dry phases of the intraseasonal oscillation. The ENSO teleconnection with the variable-length northern Australian rainy season also exhibits spatial heterogeneity and significant differences from rainfall anomalies using the fixed-length boreal winter season. The onset, the retreat, the length, and the seasonal rainfall anomalies of the rainy season display a stronger correlation with the ENSO SST anomalies for the region east of 140°E relative to its west. The strong covariability of the local onset date with the corresponding seasonal length and seasonal rainfall anomalies over northern Australia offers the advantage of monitoring the onset of the northern Australian rainy season to provide an outlook for the forthcoming season. The proposed local definition of onset/retreat of the northern Australian rainy season is simple, objective, and unambiguous and is ideally suited for real-time monitoring of the evolution of the season.

KEYWORDS: Atmosphere; Australia; ENSO; Madden-Julian oscillation

1. Introduction

The diagnosis of the onset and retreat of the northern Australian wet season has a very rich history of investigation (Lisonbee et al. 2020). As pointed out in Lisonbee et al. (2020), the northern Australian climate features a distinct dry from the wet season. The dry season extends approximately from May to September, and the wet season is from October to April. However, despite this clarity in the distinction between the two seasons, the definition of the onset and retreat of the northern Australian monsoon has been rather varied. For example, some studies refer to the shifting of the low-level winds from easterly to westerly to mark the start and the end of the monsoon season over northern Australia (e.g., Troup 1961; Holland 1986; Drosdowsky 1996). Other studies have focused on the onset and the retreat of the rains to mark the start and the end of the monsoon season over northern Australia (e.g., Nicholls et al. 1982; Nicholls 1984; Lo and Wheeler 2007; Smith et al. 2008a; Uehling and Misra 2020, hereafter UM20). Even within the monsoon season of northern Australia, a distinction is drawn between the early and later part of the season (Pope et al. 2009). In the early part of the season between October and December, rainfall patterns are categorized as isolated mesoscale thunderstorms, while in the later part of the season (January–March), the rainfall is associated with more large-scale rain systems of the northern Australia. UM20 make a subtle but important distinction between the monsoon and the rainy seasons of northern Australia with the former acknowledging the seasonal shift of the kinematic field while the latter marking the seasonal shift in rainfall. Nonetheless, UM20 points out that despite these distinctions, the northern Australian monsoon season and the rainy (or wet) season significantly overlap with each other with the latter being longer and showing more robust teleconnections with El Niño–Southern Oscillation (ENSO).

The onset and the retreat of the northern Australian wet season are also associated with the intraseasonal variability (Troup 1961; Hendon et al. 1989; Hendon and Liebmann 1990a,b; Krishnamurti et al. 1995; Wheeler and Hendon 2004). For example, some studies indicate that majority of the onset of the northern Australian monsoon season occurs during the wet phase of the Madden–Julian oscillation (MJO; e.g., Pope et al. 2009; Wheeler and McBride 2012). In this study, we will reexamine this relationship of the intraseasonal variations with the proposed new definition of local onset and local retreat of the northern Australian rainy season (NARS). In UM20 we introduced a definition of the onset and retreat of the wet season based on the area average rainfall over northern Australia. This definition had the advantage of being objective and simple (solely based on rainfall), which can be adopted operationally for real-time monitoring. In this study, however,

Corresponding author: John Uehling, juehling@fsu.edu

DOI: 10.1175/MWR-D-21-0093.1

we extend our previous work to offer a localized definition to the onset/retreat of the wet season over northern Australia that will naturally lend itself to display the spatial heterogeneity of the seasonal evolution.

In the following section, we describe the datasets used in the study, followed by a discussion of the adopted methodology in section 3. The results are discussed in section 4, followed by concluding remarks in section 5.

2. Datasets

The rainfall analysis based on the Australian Bureau of Meteorology's rain gauge network across the Australian continent (http://www.bom.gov.au/climate/how/newproducts/IDCdrgrids.shtml; Grant 2012) are the primary data used in this study. The dataset is available on a 0.5° grid over the entire Australian landmass and is available over a 114-yr period beginning on 1 January 1900 and ending on 31 December 2015 (with one year, 1958, missing). The rain gauge data are gridded using the optimized Barnes successive correction technique (Jones et al. 2009). This gridded rainfall analysis has a root-mean-square error of 3.1 mm and a mean absolute error of 0.9 mm (Grant 2012). The daily rainfall is nominally measured each day at 0900 local time. One potential limitation of using this rainfall data is that the observational network across the Australian outback is quite sparse. This study is, however, focused on northern Australia, which is north of the outback and has a higher density of rain gauges. We also make use of NOAA reconstructed SST (Smith et al. 2008b) for computing the Niño-3.4 SST index for ENSO variations.

3. Methodology

a. *Diagnosis of local onset/retreat of the northern Australian rainy season*

The onset and the retreat of the aggregate (area-averaged rainfall over northern Australia) NARS was diagnosed in UM20. The methodology used in UM20 allows for an objective and robust definition of the NARS, which is primarily based on rainfall following the methodology described in Liebmann and Marengo (2001). In the study, the daily rainfall is averaged over the northern Australian domain (all land grid points in a box defined by longitudes 120°–150°E and latitudes 20°–10°S), from which the cumulative anomaly curve [Eq. (1)] of daily rainfall is computed for each individual year:

$$A_m(n) = \sum_{n=1}^{j} \left[\bar{r}_m(n) - \bar{\bar{r}} \right], \tag{1}$$

where $A_m(n)$ is the cumulative anomaly of the area averaged precipitation for day n of year m, $\bar{r}_m(n)$ is spatially averaged rainfall over northern Australia for day n of year m, and $\bar{\bar{r}}$ is the area average and annual mean climatology of rainfall:

$$\bar{\bar{r}} = \frac{1}{MNK} \sum_{m=1}^{M} \sum_{n=1}^{N} \sum_{i=1}^{K} r(m,n,i), \tag{2}$$

where the summation over i is for area average by averaging over all K grid points over northern Australia, summation over n is averaging over all N days of the year for getting the annual mean, and the summation over m is over all M years (1901–2015) to obtain the climatology of the annual mean. It may be noted that in the summation over n in Eq. (2), $n = 1$ is 1 July of a given year and N is 30 June of the following year. The minima and maxima in the $A_m(i)$ curve correspond to aggregate NARS onset (δ) and retreat (γ) date, respectively. Such a definition marks the onset and the retreat as the first and the last day of the year when the daily rain rate exceeds and falls below the annual mean climatological rain rate, respectively.

The definition of the rainy season introduced in UM20 is, however, for the aggregate northern Australian region. In this study, we introduce a local definition for the onset/retreat of the NARS, akin to Misra et al. (2017a) used for the Indian summer monsoon. In the local definition, we define local onset/retreat of the season at every discrete grid point of the rainfall analysis over northern Australia using a similar methodology as elaborated in Eqs. (1) and (2) but applied at every grid point. However, to avoid the likelihood of detecting false onset/retreat dates on account of synoptic- or mesoscale variability that may be unrelated to the seasonal evolution, we anchor the diagnosis of the local onset and retreat dates to the climatological local onset and retreat dates following Misra et al. (2017a).

To diagnose the local onset, we first compute the climatological local onset/retreat first in the following manner.

The daily cumulative anomaly curve for day i [$lc_x(i)$] of the local daily rainfall climatology is

$$lc_x(i) = \sum_{n=1}^{i} [\bar{r}_x(n) - \bar{\bar{c}}_x], \tag{3}$$

where $\bar{r}_x$ is the climatological daily rain at grid point x for day n, and $\bar{\bar{c}}_x$ is the annual mean rainfall climatology at grid point x. The $\bar{\bar{c}}_x$ was computed using the following formula:

$$\bar{\bar{c}}_x = \frac{1}{NM} \sum_{m=1}^{M} \sum_{n=1}^{N} r(m,n)_x, \tag{4}$$

where n is the number of days in a year, and m is the number of years in total (in this case, 114). Figure 1 shows an example of how the cumulative anomaly curve can be calculated from the daily rainfall climatology for a given grid point (for instance, over Darwin, Australia). The climatological local onset $\bar{\tau}_x$ and retreat $\bar{\phi}_x$ for a grid point x is diagnosed as the minimum and the maximum in the cumulative anomaly curve (Fig. 1). The above procedure is repeated at each of the grid points of the rainfall analysis to diagnose $\bar{\tau}_x$ and $\bar{\phi}_x$ of NARS. Similarly, the local onset τ_x and retreat ϕ_x of the NARS for every year is computed but from the cumulative rainfall anomaly curve of a given year. To avoid the diagnosis of false local onset/retreat dates of the rainy season, we ensure that τ_x and ϕ_x are diagnosed as the closest minimum and maximum to $\bar{\tau}_x$ and $\bar{\phi}_x$, respectively.

b. *Diagnosis of the intraseasonal variations on the evolution of the northern Australian rainy season*

To understand the potential influence of the intraseasonal oscillations (ISOs) or the MJO on the variations of the NARS, a multichannel singular spectrum analysis

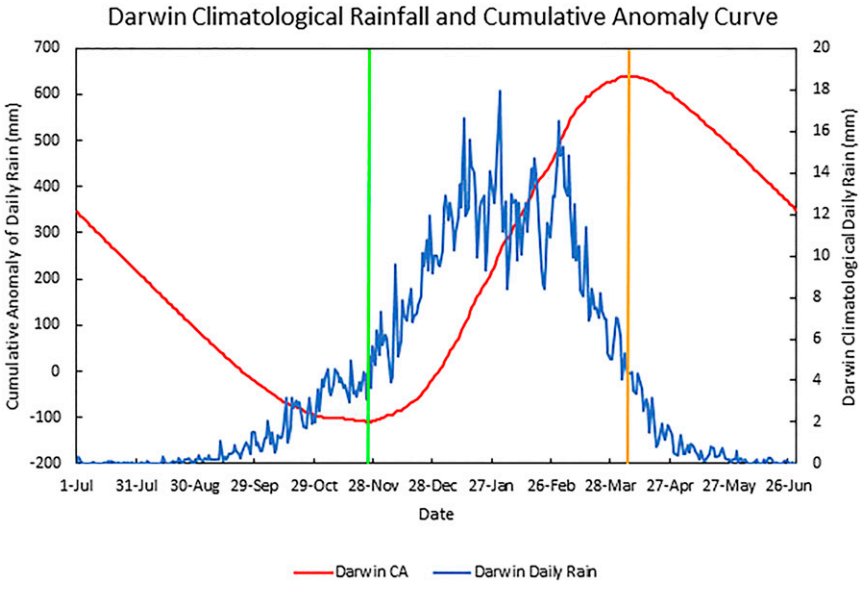

FIG. 1. Daily climatological rain rate (in blue) over Darwin (12.4°S and 130.8°E). The corresponding daily cumulative anomaly of rainfall (in red) and the diagnosed onset (indicated by the green vertical line) and retreat (indicated by the orange vertical line) dates are diagnosed by the minimum and maximum in the red curve, respectively.

(MSSA; Ghil et al. 2002) was performed. MSSA, a spatiotemporal, data-adaptive filtering technique, has been widely used for isolating intraseasonal variations (e.g., Krishnamurthy and Shukla 2007; Karmakar et al. 2017). The advantage to using the MSSA technique rather than a simpler harmonic analysis or Fourier transform is that the shape and bandwidth of the MSSA filters are themselves functions of the input data.

The input data to the MSSA are the daily rainfall anomalies after removing the daily climatology and applying a 5-day moving mean. A window length of 60 days is used to make lagged copies of the rainfall data to construct the lag-covariance matrix that is diagonalized to obtain space–time empirical orthogonal functions (EOFs) and principal components (PC). Oscillations in the bandwidth of 30–60 days is isolated if the associated eigenvalues are nearly equal and the phase of the two EOFs are in quadrature.

Using the MSSA technique, the phase composites of the ISO are computed for each year from 1900/01 to 2014/15. Only the rainfall data from the time surrounding and including the NARS were used [from Julian day 290 (17 October) to Julian day 120 (30 April) of the following year], rather than for the entire year. This ensures that the signals that are originating from ISOs during the rainy season were isolated. The sinusoidal oscillations of the ISO are divided into eight phases following Karmakar and Misra (2020). The first four phases of the ISO will be nearly opposite in phase to the following four phases. These phases are computed to develop corresponding composites to understand the evolution of the NARS in relation to the propagation of the ISO.

To examine the statistical significance of some of our results we use the nonparametric bootstrapping technique for statistical significance (Wilks 2011). This has been widely used for significance tests (e.g., Mo 2010; Yuan et al. 2015; Misra et al. 2017b).

4. Results

a. Climatological local onset/retreat of the northern Australian rainy season

The onset/retreat dates of the NARS are computed for 114 years at every land grid point of the domain. The red curve in Fig. 1 shows the climatological cumulative rainfall anomaly curve over Darwin (12.4°S and 130.8°E), with the minima of the curve being the onset date and the maxima being the retreat date of the rainy season. Climatologically, the onset date of the rainy season over Darwin occurs on Julian day 329 (~25 November), whereas the climatological retreat date over Darwin is around Julian day 98 (~8 April of the following year). It can also be seen that the definition used for calculating the local rainy season over Darwin corresponds to the period of highest rainfall during the year (Fig. 2).

Figures 2a and 2b show the spatial distribution of the local climatological onset and retreat dates of NARS, respectively. It is noteworthy that the evolution of NARS varies markedly across the domain (Figs. 2a,b). Figure 3a shows that the onset of NARS begins in the western portion of northern Australia earlier than in the eastern portion (Fig. 2a). The earliest onset dates on average, occur in the northern Territories of northern Australia in a band around 130°E longitude. The onset generally occurs in this band around the 315th–325th Julian day of the year. The land areas to the west of the Gulf of Carpentaria generally have earlier onsets than land areas to

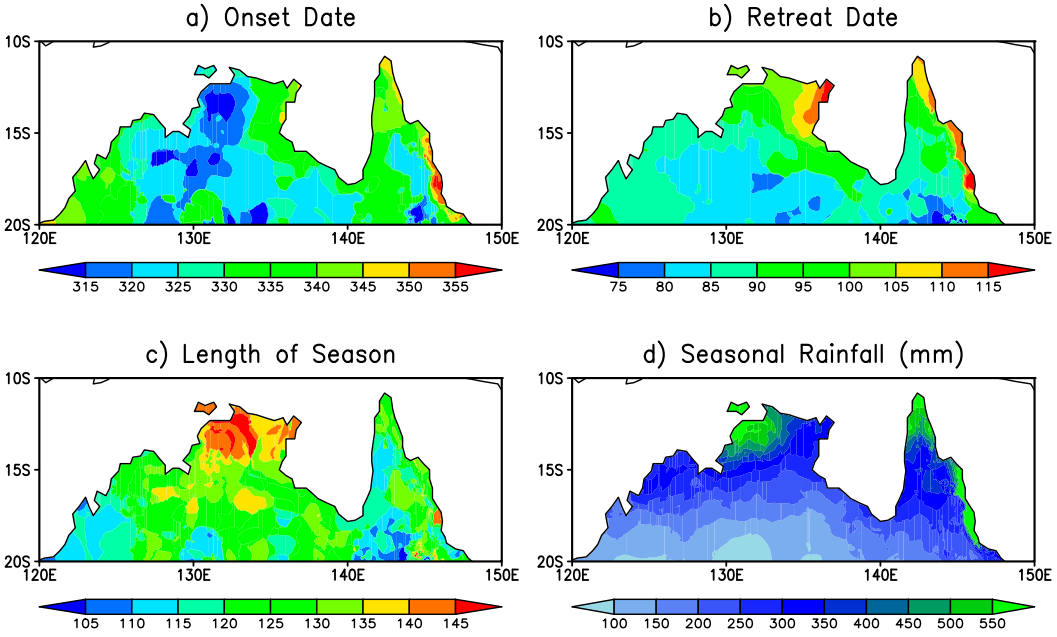

FIG. 2. The climatological (a) onset and (b) retreat date (in Julian days), and (c) length (in days) of the NARS defined at every grid point of the Australian Bureau of Meteorology gridded rainfall dataset at a 0.5° grid interval (Grant 2012). (d) The climatological seasonal mean rainfall (mm), accumulated between the climatological local onset and retreat date of the NARS at each grid point.

the east and south of the Gulf of Carpentaria (Fig. 2a). In the eastern part of northern Australia, the average onset date of the rainy season ranges between the 330th and 350th days of the year (Fig. 2a).

Similarly, Fig. 2b shows the spatial distribution of the climatological local retreat dates of the NARS. The spatial distribution of the climatological retreat date of the rainy season reflects the ''lifting out'' of the monsoon trough over northern Australia. As the monsoon season draws to a close, the contrast between the ocean and land temperatures reduces as the monsoon trough moves to the north away from the Australian continent. This is reflected in Fig. 2b, which shows the earliest retreat dates on average occurring to the south and the latest retreat dates occurring in the northernmost regions of northern Australia (Fig. 2b). It may be noted that the monsoon trough generally appears to translate out of the region from southwest to northeast, as the retreat dates occur later in the season, moving from southwest to northeast.

Figures 2c and 2d show the climatological seasonal length of NARS for each grid point, as well as the climatological seasonal rainfall that accounts for the changing length of the season, respectively. The length of the rainy season generally increases from south to north. This follows from the monsoon trough appearing in each season by moving south over the region and then lifting back out meridionally toward the end of the season. It may be noted that the region just to the west of the Gulf of Carpentaria exhibits the earliest and the latest climatological onset and retreat dates, which results in the longest climatological rainy seasons over northern Australia (Fig. 2c). This region has rainy seasons that last on average longer than 140 days. Most of the rest of northern Australia experiences rainy seasons that last on average around 115–130 days (Fig. 2c). Figure 2d shows the northernmost regions of Australia receiving the most rainfall, with a general progression

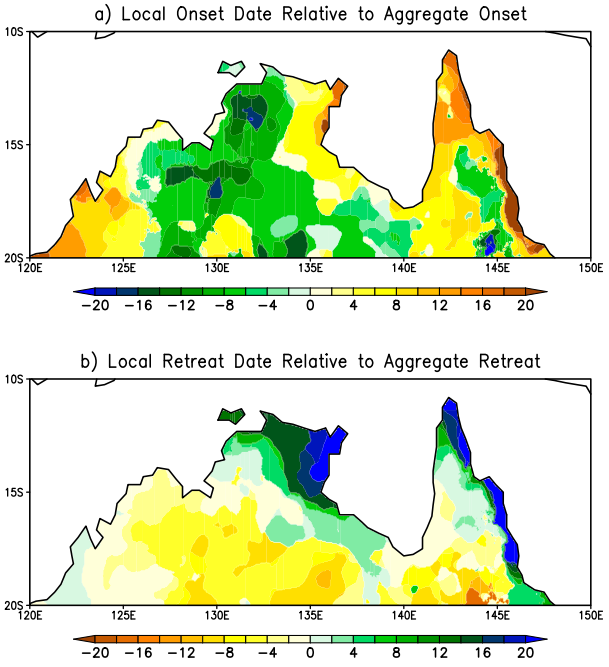

FIG. 3. The difference of the climatological date of (a) local onset from the onset date of the aggregate NARS and (b) local retreat from the retreat date of the aggregate NARS.

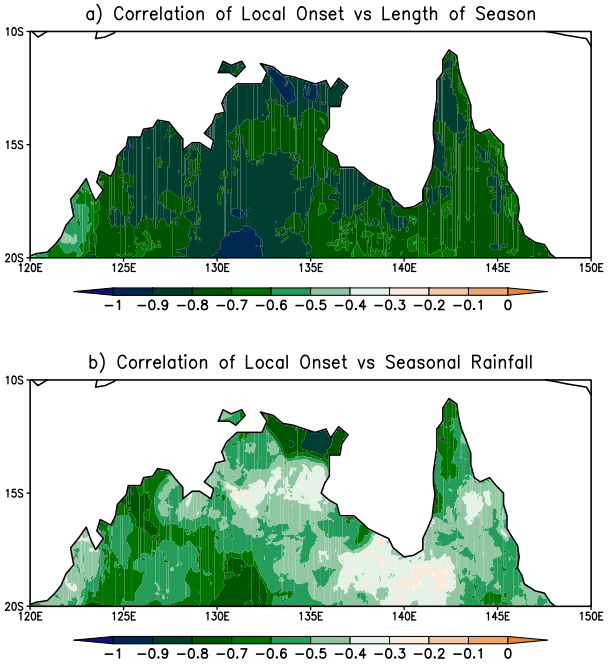

FIG. 4. The correlation of the local onset date of NARS with corresponding (a) local length of the NARS and (b) local seasonal rainfall anomaly of NARS. Only significant values at 5% significance level by the bootstrap method are shaded.

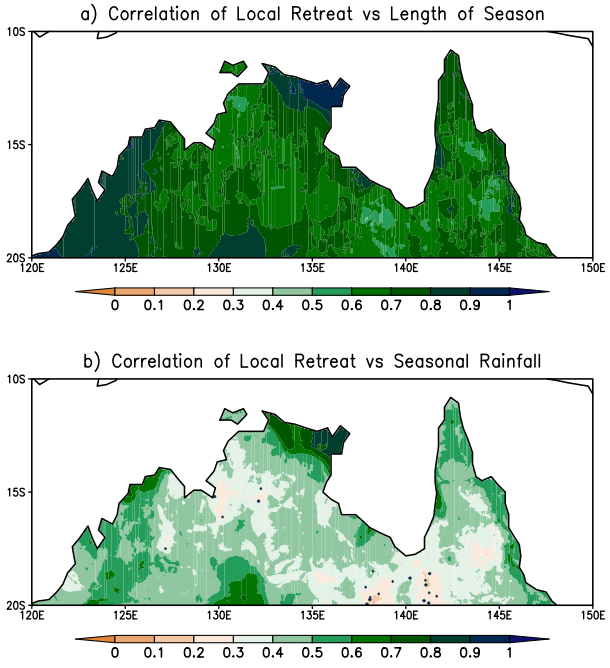

FIG. 5. The correlation of the local retreat date of the NARS with corresponding (a) local length of the NARS and (b) local seasonal rainfall anomaly. Only significant values at 5% significance level by the bootstrap method are shaded.

of less rainfall as one moves further south toward the Australian interior. Near the northern and eastern coasts of northern Australia, climatological rainy season rainfall averages over 500 mm per season. These values decrease as one moves south to the southern reaches of the domain, with the climatological seasonal rain reaching around 100–200 mm per season.

Figures 3a and 3b show the progression of the climatological local onset and local retreat with respect to the aggregated NARS onset and retreat dates, respectively. In Fig. 3a, we see that the earliest climatological local onsets occur nearly 10 days before the climatological onset of the aggregate NARS in the northern tip of the Northern Territory and the northeastern tip of the Western Australia. Then the climatological local onset slowly progresses eastward and southward before a majority of northern Australia attains its climatological local onset by around 8 days after the aggregate NARS climatological onset (Fig. 3a). Furthermore, by day 19, after the climatological onset of the aggregate NARS onset, the remaining portion of the horn of Australia also achieves its climatological local onset (Fig. 3a). Similarly, the climatological local retreat date appears first along the southern tip of the northern Australian domain almost 10 days before the climatological retreat date of the aggregate NARS is reached (Fig. 3b). The climatological local retreat date then slowly progresses northward before all of the domain attains the climatological retreat by the 19th day after the climatological retreat of the aggregate NARS is reached. In comparing Figs. 3a and 3b it can be noted that the spatial distribution of the climatological onset and the retreat dates of NARS is largely symmetrical, with earlier and later onset regions corresponding to later and earlier retreat of the season. However, the climatological local onset dates exhibit a stronger zonal gradient (Fig. 3a) while the climatological local retreat dates display a stronger meridional gradient (Fig. 3b).

b. Interannual variability

There is a strong relationship between the variations of the local onset date and the local seasonal length of NARS (Fig. 4a). The negative correlations between the onset date and the seasonal length in Fig. 4a suggest that earlier or later onset date at a given grid point is associated with longer or shorter rainy season, respectively. Figure 4a shows the strongest negative correlations are in the northern part of Australia, which is also the region with the earliest onset dates in the domain (Fig. 2a). Similarly, Fig. 4b shows the correlation between the local onset date and the corresponding seasonal rainfall anomaly. This figure demonstrates that there is a generally strong negative correlation between the onset date and the seasonal rainfall anomaly, suggesting that early or later onset is associated with wetter or drier rainy season, respectively. Therefore, Figs. 4a and 4b strongly suggest that monitoring the variability of the local onset date of the rainy season over northern Australia can serve as a good seasonal outlook for the following rainy season in terms of its seasonal length and seasonal rainfall anomaly.

Figures 5a and 5b show the correlations of the variations of the retreat date with the seasonal length and seasonal rainfall anomalies of NARS, respectively. The correlations in Figs. 5a

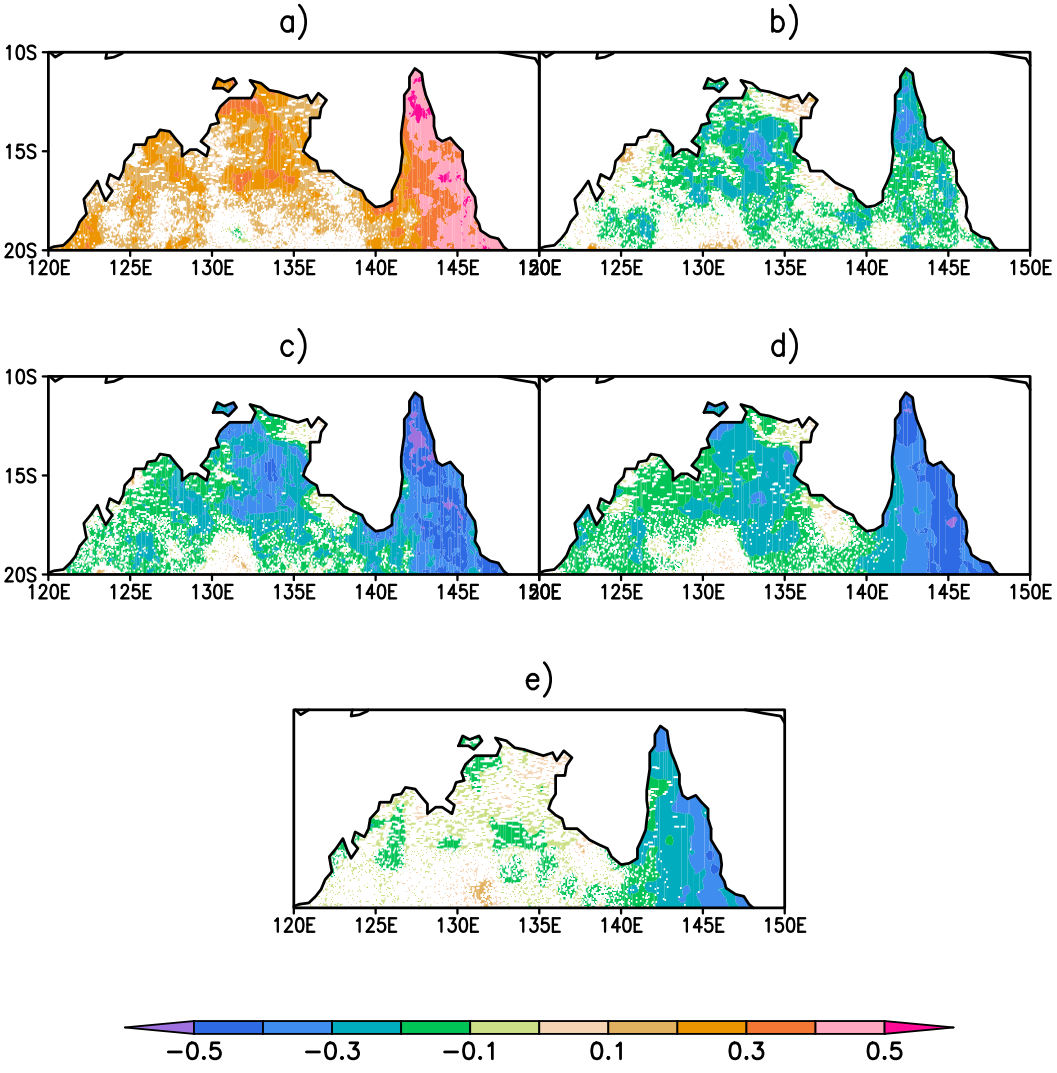

FIG. 6. The correlation of September–November (SON) seasonal mean Niño-3.4 (ENSO) SST anomalies with (a) local onset date, (b) local retreat date, (c) local seasonal length, (d) local seasonal rainfall anomalies, and (e) fixed-length December–February (DJF) seasonal rainfall anomalies of NARS. All correlations significant at 95% confidence interval according to the bootstrap method are shaded.

and 5b are positive, suggesting that early or later retreat of the rainy season is associated with shorter and drier or longer and wetter rainy season, respectively. Figures 5a and 5b suggest that monitoring the retreat date variations of NARS could be useful to posteriorly analyze the season. Interestingly, the correlations between the local onset and the corresponding local retreat date variations are statistically insignificant (not shown).

The ENSO teleconnection with NARS is significant (Holland 1986; UM20). UM20 showed that this teleconnection becomes stronger when the variations of the length of the aggregated NARS are considered. Figure 6a shows that there is a strong positive correlation between the September–November (SON) seasonal mean Niño-3.4 (ENSO) SST anomalies and the local onset date suggesting that warm or cold ENSO SST anomalies are associated with later or early local onset of NARS, respectively. This relationship tends to be strongest east of the Gulf of Carpentaria (east of 140°E; Fig. 6a). The opposite relationship is shown between the SON seasonal mean ENSO SST anomalies and the local retreat date of NARS (Fig. 6b). The correlations between Niño-3.4 SST anomalies and the corresponding retreat date variations are, however, weaker (Fig. 6b) relative to variations with the onset date variations (Fig. 6a). This relationship also manifests in and is reflected by the negative correlation between the SON seasonal mean ENSO SST anomalies and the local seasonal length variations (Fig. 6c). The correlation in Fig. 6c implies that warm or cold SON seasonal mean ENSO SST anomalies are associated with shorter or longer seasonal length of the rainy season over northern Australia, respectively. Again, the variability between the ENSO SST anomalies and seasonal length are comparatively stronger to the east of Gulf of Carpentaria (Fig. 6c). Finally,

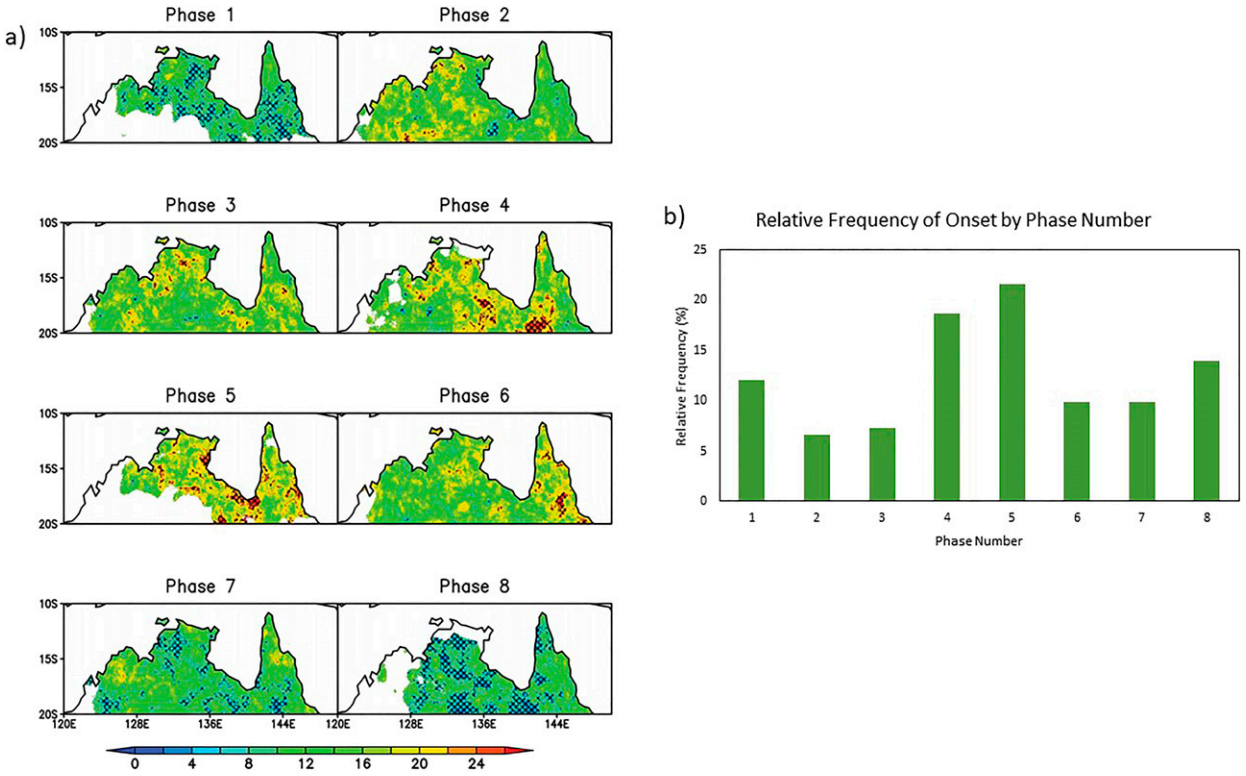

FIG. 7. (a) Spatial distribution of the frequency of local onset dates of NARS occurring in of the eight phases of ISO across northern Australia. The hatched regions indicate statistically significance at 5% significance level by the bootstrap method. (b) Histogram showing the relative frequency (percentage) of local onset dates of NARS occurring during each phase of the ISO. The frequency is computed only in statistically significant regions [hatched regions in (a)].

the correlations between the SON Niño-3.4 SST anomalies and seasonal rainfall anomaly (Fig. 6d) nearly mimic the correlations with seasonal length (Fig. 6c), suggesting that warm or cold ENSO anomalies are associated with the drier or wetter season. In comparison, the correlations of the SON ENSO SST anomalies with fixed length December–February seasonal rainfall anomalies over northern Australia are largely confined to east of 140°E (Fig. 6e). The comparison of Figs. 6d and 6e clearly illustrate the importance of accounting for the spatial heterogeneity of NARS. More importantly, we conclude that acknowledging the variations of the local seasonal length of NARS in computing the seasonal rainfall anomaly is critical to diagnose the ENSO teleconnections over the region.

c. *Intraseasonal variations*

By utilizing the MSSA methodology described previously, rainfall phase composites of the ISO rainfall during November–May 1900–2015 were generated. These phase composites reveal that during the first four phases of the ISO, on average, there is enhanced precipitation over the northern Australian domain, suggesting a wet spell while the remaining four phases represent the dry spell (not shown). A spatial distribution of the frequency of the local onset and retreat dates of NARS in each of the eight phases of the ISO is shown in Fig. 7. The largest density of local onset of NARS occurs around the Gulf of Carpentaria in phases 4 and 5 of the ISO (Fig. 7a). In the first four (wet) phases of the ISO, the frequency of local onset is lower (44.65%) than in the latter four (dry) phases of the ISO. This feature is also illustrated by the relative frequency (= number of onset in each phase in statistically significant/total number of local onsets in all phases in statistically significant regions) in Fig. 7b. Figure 7b indicates that most local onset occurs in the wet spell phases of 1 and 4 of the ISO and in phases 5 and 8 of the dry spell of the ISO. We observe from the spatial distribution of local onsets in Fig. 7a that there is no coherent pattern of local onset occurring in the wet and dry spells of the ISO to suggest that one region of the domain is more conducive than the other for local onsets to occur in the wet/dry phases of the ISO.

Similarly, the spatial distribution of the frequency of the local retreat date within the different phases of the ISO is shown in Fig. 8a. We observe that some of the highest density of local retreat occurs in phases 7 and 8 of the ISO, while in the remaining phases of the ISO the frequency of local retreat is more uniform across the domain (Fig. 8b). In contrast to the frequency of local onset, the local demise of NARS occurs 71.31% in the dry spells (phases 5–8) of the ISO. We find from Fig. 8a that most of the local demise of NARS during dry spell of the ISO occurs around the Gulf of Carpentaria and in the southeast region of the domain. The southwest region of the domain uniquely exhibits a high density of local demise of NARS during Phase 3 (wet spell) of the ISO.

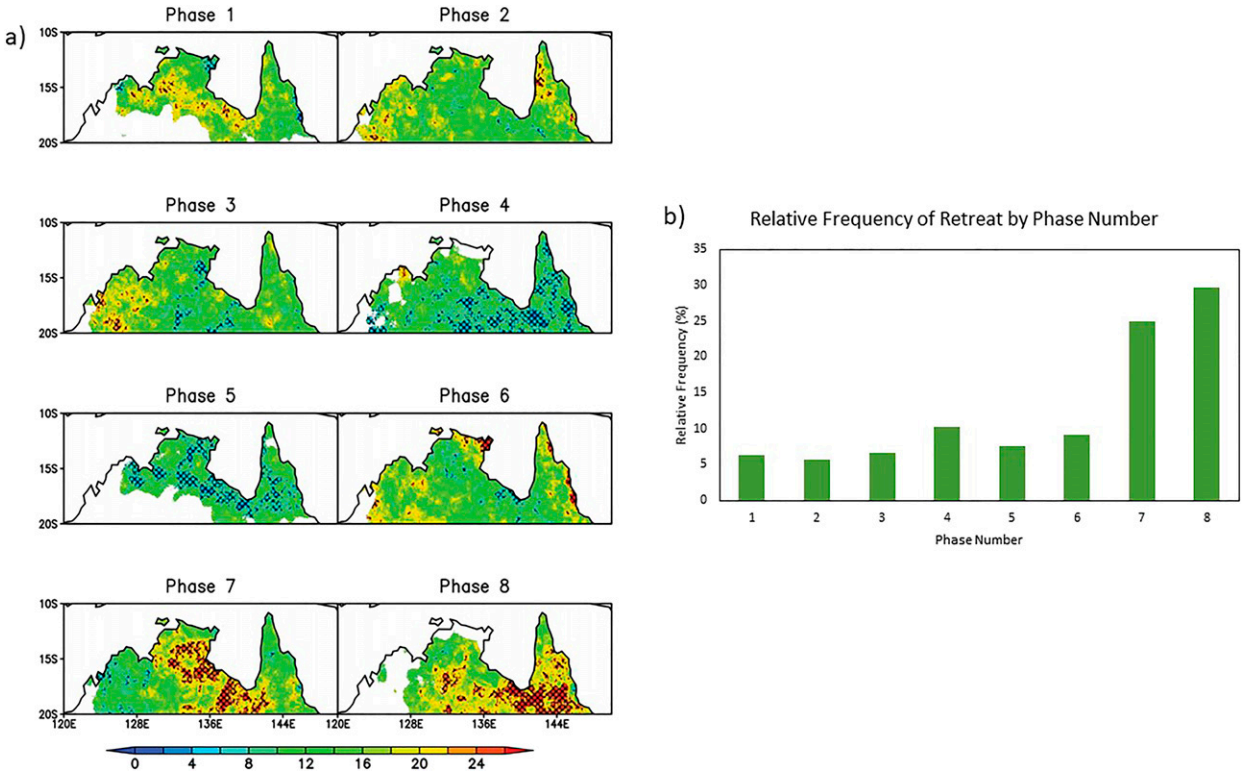

FIG. 8. (a) Spatial distribution of the frequency of local retreat dates of NARS occurring in each phase of the ISO across northern Australia. The hatched regions indicate statistically significance at 5% significance level by the bootstrap method. (b) Histogram showing the relative frequency (percentage) of local retreat dates of NARS occurring during each phase of the ISO. The frequency is computed only in statistically significant regions [hatched regions in (a)].

5. Conclusions

The local definition of NARS, as introduced in this paper, is an attractive complement to the aggregate evolution of NARS in UM20. The spatial heterogeneity observed in the evolution of the rainy season over northern Australia with early onsets and longer length of the season occurring to the west of Gulf of Carpentaria necessitates a local definition for the onset and the retreat of NARS.

The local definition of onset/retreat of NARS is based on daily rainfall analysis, which is defined at individual grid points. This definition requires a robust seasonal cycle of rainfall so that onset and retreat can be defined as the first and the last day of the year when the daily rain rate exceeds and falls below the climatological annual mean rain rate. However, to avoid false onset/retreat dates that are not associated with the rainy season, we anchor our local definition of onset/retreat to the climatological evolution of the local rainy season with respect to the corresponding aggregate NARS evolution. This local definition provides an unambiguous, objective definition of the onset/retreat of NARS defined locally, at the individual grid points of the rainfall analysis.

The proposed definition of local onset/retreat NARS has many advantages. Foremost it accounts for local variations in the length of the season, which is an important variant of the season. Second, it is based solely on rainfall, which makes it convenient to implement in case of real-time monitoring of the season. We tested this methodology over a century-long rainfall analysis, which showed the efficacy of this objective definition in providing unambiguous local onset/retreat dates throughout the period. In the future, this definition could be adopted on remotely sensed rainfall products that are available on shorter periods of time at potentially higher spatial resolution and available in real time. Furthermore, the introduced methodology for diagnosing local onset and retreat of NARS is easily adaptable to the available resolution of the rainfall analysis.

Our study finds that local onset/retreat variations have an implication on the corresponding length of the season and seasonal rainfall anomaly. We find that early or later local onset of the rainy season is associated with longer and wetter or shorter and drier seasons, respectively. This relationship can be exploited to provide a localized seasonal outlook of the rainy season by monitoring the local onset. Similarly, the linear relationship of the variations of the local retreat of the season with the corresponding length of the season and seasonal rainfall anomaly provides an understanding of the local evolution of the season posteriorly.

The frequency of the local onset and retreat of NARS is prominent in the wet and dry phases of the ISO, respectively. There is a far greater frequency of local demise (71.31%) during the dry spells of the ISO relative to the wet spells of the ISO. However, the frequency of local onset during wet spells of

the ISO is 44.65%, which is less than the local onset occurring in the dry spells of the ISO. This observation is intriguing but nonetheless important to note, while future studies examine the subseasonal predictability of the evolution of NARS. The spatial distribution of the frequency of local demise of NARS during the various phases of the ISO exhibit coherent areas of high frequency during dry phases of ISO around the Gulf of Carpentaria. However, such spatial patterns are less discerning with regard to local onsets of NARS and ISO phases.

The ENSO teleconnections show that there is a strong relationship with the local variations of NARS. Early local onset, later local retreat, longer local length, and local wetter rainy season anomalies are associated with negative ENSO Niño-3.4 SST anomalies. Likewise, later onset, early local retreat, shorter local length, and local drier rainy seasonal anomalies are associated with positive ENSO SST anomalies. These teleconnections exhibit some spatial heterogeneity, with the eastern part of northern Australia exhibiting stronger correlations with ENSO Niño-3.4 SST anomalies than the regions to the west of 140°E. Furthermore, in comparison to the fixed-length seasonal rainfall anomalies of DJF, the correlations with ENSO Niño-3.4 SST anomalies with locally varying length of NARS rainfall anomalies display a stronger and more widespread correlation to the west of 140°E over northern Australia. This suggests that the seasonal predictability of NARS with a variable seasonal length in relation to its variation with ENSO could be potentially exploited further than by using a fixed-length season of NARS.

Acknowledgments. This work is supported by NASA Grant NNX17AG72G.

Data availability statement. The datasets are available from public repositories cited in the text.

REFERENCES

Drosdowsky, W., 1996: Variability of the Australian summer monsoon at Darwin: 1957–1992. *J. Climate*, **9**, 85–96, https://doi.org/10.1175/1520-0442(1996)009<0085:VOTASM>2.0.CO;2.

Ghil, M., and Coauthors, 2002: Advanced spectral methods for climatic time series. *Rev. Geophys.*, **40**, 31–341, https://doi.org/10.1029/2000RG000092.

Grant, I., 2012: Daily Rain Gauge Precipitation (Rainfall) - Gridded, Australia coverage. Bureau of Meteorology, accessed December 2014, http://data.auscover.org.au/xwiki/bin/view/Product+pages/Product+User+Page+Melbourne+2.

Hendon, H. H., and B. Liebmann, 1990a: A composite study of onset of the Australian summer monsoon. *J. Atmos. Sci.*, **47**, 2227–2240, https://doi.org/10.1175/1520-0469(1990)047<2227:ACSOOO>2.0.CO;2.

——, and ——, 1990b: The intraseasonal (30–50 day) oscillation of the Australian summer monsoon. *J. Atmos. Sci.*, **47**, 2909–2924, https://doi.org/10.1175/1520-0469(1990)047<2909:TIDOOT>2.0.CO;2.

——, N. E. Davidson, and B. Gunn, 1989: Australian summer monsoon onset during AMEX 1987. *Mon. Wea. Rev.*, **117**, 370–390, https://doi.org/10.1175/1520-0493(1989)117<0370:ASMODA>2.0.CO;2.

Holland, G. J., 1986: Interannual variability of the Australian summer monsoon at Darwin: 1952–82. *Mon. Wea. Rev.*, **114**, 594–604, https://doi.org/10.1175/1520-0493(1986)114<0594:IVOTAS>2.0.CO;2.

Jones, D. A., W. Wang, and R. Fawcett, 2009: High-quality spatial climate datasets for Australia. *Aust. Meteor. Oceanogr. J.*, **58**, 233–248, https://doi.org/10.22499/2.5804.003.

Karmakar, N., and V. Misra, 2020: The fidelity of a regional coupled model in capturing the relationship between intraseasonal variability and the onset/demise of the Indian summer monsoon. *Climate Dyn.*, **54**, 4693–4710, https://doi.org/10.1007/s00382-020-05252-z.

——, A. Chakraborty, and R. S. Nanjundiah, 2017: Space-time evolution of the low- and high-frequency intraseasonal modes of the Indian Summer Monsoon. *Mon. Wea. Rev.*, **145**, 413–435, https://doi.org/10.1175/MWR-D-16-0075.1.

Krishnamurthy, V., and J. Shukla, 2007: Intraseasonal and seasonally persisting patterns of Indian monsoon rainfall. *J. Climate*, **20**, 3–20, https://doi.org/10.1175/JCLI3981.1.

Krishnamurti, T. N., S. K. Han, and V. Misra, 1995: Predictions of dry and wet spells of the Australian monsoon. *Int. J. Climatol.*, **15**, 753–771, https://doi.org/10.1002/joc.3370150704.

Liebmann, B., and J. Marengo, 2001: Interannual variability of the rainy season and rainfall in the Brazilian Amazon basin. *J. Climate*, **14**, 4308–4318, https://doi.org/10.1175/1520-0442(2001)014<4308:IVOTRS>2.0.CO;2.

Lisonbee, J., J. Ribbe, and M. Wheeler, 2020: Defining the north Australian monsoon onset: A systematic review. *Prog. Phys. Geogr.*, **44**, 398–418, https://doi.org/10.1177/0309133319881107.

Lo, F., and M. C. Wheeler, 2007: Probabilistic forecasts of the onset of the north Australian wet season. *Mon. Wea. Rev.*, **135**, 3506–3520, https://doi.org/10.1175/MWR3473.1.

Misra, V., A. Mishra, and A. Bhardwaj, 2017a: Local onset and demise of the Indian summer monsoon. *Climate Dyn.*, **51**, 1609–1622, https://doi.org/10.1007/s00382-017-3924-2.

——, A. Bhardwaj, and R. Noska, 2017b: Understanding the variations of the length and the seasonal rainfall anomalies of the Indian summer monsoon. *J. Climate*, **30**, 1753–1763, https://doi.org/10.1175/JCLI-D-16-0501.1.

Mo, K. C., 2010: Interdecadal modulation of the impact of ENSO on precipitation and temperature over the United States. *J. Climate*, **23**, 3639–3656, https://doi.org/10.1175/2010JCLI3553.1.

Nicholls, N., 1984: A system for predicting the onset of the north Australian wet season. *J. Climatol.*, **4**, 425–435, https://doi.org/10.1002/joc.3370040407.

——, J. L. McBride, and R. J. Ormerod, 1982: On predicting the onset of the Australian wet season at Darwin. *Mon. Wea. Rev.*, **110**, 14–17, https://doi.org/10.1175/1520-0493(1982)110<0014:OPTOOT>2.0.CO;2.

Pope, M., C. Jakob, and M. J. Reeder, 2009: Regimes of the north Australian wet season. *J. Climatol.*, **22**, 6699–6715, https://doi.org/10.1175/2009JCLI3057.1.

Smith, I. N., L. Wilson, and R. Suppiah, 2008a: Characteristics of the northern Australian rainy season. *J. Climate*, **21**, 4298–4311, https://doi.org/10.1175/2008JCLI2109.1.

Smith, T. M., R. W. Reynolds, T. C. Peterson, and J. Lawrimore, 2008b: Improvements to NOAA's historical merged land-ocean surface temperature analysis (1880–2006). *J. Climate*, **21**, 2283–2296, https://doi.org/10.1175/2007JCLI2100.1.

Troup, A. J., 1961: Variations in upper tropospheric flow associated with the onset of the Australian monsoon. *Indian J. Meteor. Geophys.*, **12**, 217–230.

Uehling, J., and V. Misra, 2020: Characterizing the seasonal cycle of the northern Australian rainy season. *J. Climate*, **33**, 8957–8973, https://doi.org/10.1175/JCLI-D-19-0592.1.

Wheeler, M. C., and H. H. Hendon, 2004: An all-season realtime multivariate MJO index: Development of an index for monitoring and prediction. *Mon. Wea. Rev.*, **132**, 1917–1932, https://doi.org/10.1175/1520-0493(2004)132<1917:AARMMI>2.0.CO;2.

——, and J. L. McBride, 2012: Australasian monsoon. *Intraseasonal Variability in the Atmosphere–Ocean Climate System*, 2nd ed. W. K. M. Lau and D. E. Waliser, Eds., Springer, 147–197.

Wilks, D. S., 2011: *Statistical Methods in the Atmospheric Sciences*. 3rd ed. International Geophysics Series, Vol. 100, Academic Press, 676 pp.

Yuan, J., W. Li, and Y. Deng, 2015: Amplified subtropical stationary waves in boreal summer and their implications for regional water extremes. *Environ. Res. Lett.*, **10**, 104009, https://doi.org/10.1088/1748-9326/10/10/104009.